

# Contrast-enhanced ultrasound (CEUS) follow-up after radiofrequency ablation or cryoablation of focal liver lesions: treated-area patterns and their changes over time

Aymeric Guibal · Caroline Bertin · Sophie Egels · Eric Savier · Philippe A. Grenier · Olivier Lucidarme

Received: 17 April 2012 / Revised: 23 September 2012 / Accepted: 12 October 2012 / Published online: 9 November 2012  
© European Society of Radiology 2012

## Abstract

**Objectives** To describe the early patterns of liver lesions successfully treated with radiofrequency ablation (RFA) or cryoablation (CA) and their changes over time.

**Methods** Twenty-two RFA-treated and 17 CA-treated patients underwent CEUS from week 1 to year 3 post-ablation. Patterns, margins and volumes of RF-induced and cryolesions were evaluated and compared over time.

**Results** After contrast enhancement, shortly after ablation, undefined margins with persistent enhancing small vessels penetrating >2 mm into the treated zone were significantly more frequent after CA (67 %) than RFA (22 %) ( $P<0.02$ ). During the arterial phase, a thin, enhancing marginal rim was seen during week 1 (T1) in around 28 % of RF lesions, while 75 % of cryolesions had thick enhancing rims ( $P<0.02$ ). The mean RF-induced lesion volume, maximum at T1 ( $44.1\pm 37.5$  ml), shrank slowly over time, remaining clearly visible at 1 year ( $8.3\pm 7.4$  ml). Cryolesions shrank faster ( $P=0.009$ ), from an average of  $16.6\pm 7.1$  ml at T1 to  $1.7\pm 1.3$  ml 1-year post-ablation.

**Conclusion** RF-induced and cryolesions differ, particularly their margins and shrinkage rates. Knowing these differences allows avoidance of incomplete treatment or falsely diagnosed recurrence, especially after CA.

## Key Points

- Contrast-enhanced ultrasound (CEUS) provides new follow-up information following hepatic radiological intervention.
- CEUS provides good visualisation of vascular modifications after thermoablation.
- RFA-induced lesions and cryoablated lesions differ.
- Knowledge about RF and cryolesion patterns is essential for correct CEUS follow-up.
- Cryolesions have thicker peripheral inflammatory reactions and shrink faster than RFA-induced lesions.

**Keywords** Cryoablation · Pulsed radiofrequency treatment · Ultrasonography · Microbubbles · Liver neoplasms

## Abbreviations

CPS	Cadence™ contrast pulse sequencing
CT	Computed tomography
CEUS	Contrast-enhanced ultrasound
CA	Cryoablation
HCC	Hepatocellular carcinoma
MRI	Magnetic resonance imaging
RFA	Radiofrequency ablation
US	Ultrasound

## Introduction

When patients are unable to undergo curative surgical resection, primary and secondary hepatic tumours can be treated with thermoablative techniques. Among them, radiofrequency ablation (RFA) and cryoablation (CA) were proven to have good long-term results for the treatment of primary or secondary liver cancers [1–5]. The radiological

A. Guibal · C. Bertin · S. Egels · E. Savier · P. A. Grenier · O. Lucidarme (✉)  
Radiology Department, Hôpital Pitié–Salpêtrière, AP–HP, Institut Universitaire de Cancérologie, University Pierre et Marie Curie (UPMC), 47–83, Boulevard de l’Hôpital, 75651 Paris cedex 13, France  
e-mail: olivier.lucidarme@psl.aphp.fr

follow-up looking initially for incomplete ablation and later for local recurrence usually consists of contrast-enhanced computed tomography (CECT) or magnetic resonance imaging (MRI). Thermoablation-induced necrosis appears on those images as a homogeneously unenhancing devascularised area. Focal peripheral enhancement on hepatic arterial-phase images is suggestive of residual hepatocellular carcinoma (HCC), whereas assessment of residual hypovascular metastases relies more on the analysis of the necrosis volume, which should exceed that of the original nodules [6, 7].

CEUS allows continuous real-time imaging of contrast enhancement during arterial, portal and late phases, and could be proposed alternately with CT or MRI to reduce ionising irradiation and costs [8, 9]. Microbubble contrast agents have a true blood-pool distribution and CEUS has high sensitivity to contrast agents, giving it the ability to visualise both the macro- and microcirculations in the tissues. Thus, CEUS should recognise successful thermoablation as the absence of contrast uptake, while residual HCC and liver metastases should exhibit nodular or crescentic contrast uptake followed by a washout in the treated area [10].

However, comparison studies with CECT or MRI did not show CEUS to have better sensitivity to incomplete ablation or later local recurrence, with false-negative and false-positive results [9, 11, 12]. Those disappointing results, particularly early after the procedure [9, 11], could be explained by the high CEUS sensitivity to the presence of microbubbles in the capillary bed, giving the treated zone a different pattern than CT or MRI. To the best of our knowledge, no complete description of the evolution of CEUS-assessed pattern over time in the areas successfully treated with RFA (henceforth called RF lesion) has been published. Concerning CA, to date, no follow-up studies using CEUS have been published and the CEUS pattern of the CA-treated area (hereafter called cryolesion) has never been described.

The primary objective of our study was to describe the early CEUS patterns of RF lesions and cryolesions after successful thermoablation and their changes over time in order to better define the spectrum of findings that can be encountered in the absence of residual tumour or local recurrence in cirrhotic and non-cirrhotic livers. The secondary goal was to compare post RFA and CA CEUS images to identify possible differences.

## Materials and methods

### Patients

This retrospective, single-centre study was part of a large multicentre study (unpublished observations) designed to

compare RFA versus CA for the treatment of primary or secondary liver tumours. It was approved by our institution's ethics committee and the patients gave their informed consent. Exclusion criteria were advanced liver disease (Child C), tumours >50 mm in diameter, with >5 liver lesions, previous local treatment in the same area and regional chemoembolisation. CT was the follow-up technique designated by the protocol and CEUS was facultative and performed only after the procedure (except for six patients who underwent pre-procedure CEUS). In our centre, between September 2004 and September 2007, 42 non-consecutive patients with 57 hepatic tumours (34 patients with and 8 patients without chronic hepatitis had 48 HCCs and 9 metastases), randomly selected for RFA ( $n=38$  tumours) or CA ( $n=19$  tumours), underwent at least two CEUS during follow-up. CEUS use was not motivated by a clinical problem but was regularly performed when the patient agreed. CECT was the gold standard to depict initial incomplete ablation or later local or distant recurrences.

In September 2010, after 3–6 years of follow-up, patients with no CT-detected incomplete thermoablation or local recurrences were declared successful. Thus, 36 patients [28 men and 8 women; mean age: 67.9 (range 49–83) years] were selected for this study and their CEUS images were reviewed. Table 1 describes the population and the lesions studied. HCCs were biopsy-proven ( $n=3$ ) or confirmed by characteristic imaging findings according to the criteria established by the European Association for the Study of the Liver Barcelona conference [13], combined with the serum alpha-fetoprotein concentration. Chronic hepatitis was due to C ( $n=10$ ) or B virus ( $n=2$ ), alcohol abuse ( $n=12$ ), hemochromatosis ( $n=2$ ) or non-alcoholic steatohepatitis ( $n=3$ ). Metastases were diagnosed based on suggestive imaging and follow-up. Five metastases originated from colorectal cancers, one from leiomyosarcoma of the inferior vena cava, one from cholangiocarcinoma and one from a neuroendocrine tumour.

### Thermoablation procedures

All thermoablation procedures were performed under general anaesthesia by the same operator (E.S.), who had 10 and 2 years of experience (at the beginning of the study) with RFA and CA, respectively. RFA and CA were performed percutaneously under US guidance (Katana, Toshiba Medical Co., Tokyo, Japan) for all but three patients who were treated after laparotomy. For both procedures, hepatic blood flow was not interrupted.

The RFA system was a 460-kHz generator unit (RF2000; Boston Scientific, Boston, MA). A 3.5-cm 15-gauge expandable 10-hook needle electrode (LeVeen needle, Radio-Therapeutics Co., Sunnyvale, CA) was used. Overlapping tumour zones were treated [14, 15] using several

**Table 1** Characteristics of the study population

Parameter	RFA		CA		Total	
	Patients, <i>n</i>	Lesions, <i>n</i>	Patients, <i>n</i>	Lesions, <i>n</i>	Patients, <i>n</i>	Lesions, <i>n</i>
Chronic hepatitis	18	27	11	14	29	41
HCC	17	26	11	14	28	40
Metastasis	1	1	0	0	1	1
No chronic hepatitis	4	4	3	4	7	8
HCC	0	0	0	0	0	0
Metastasis	4	4	2	3	6	7
Cholangiocarcinoma	0	0	1	1	1	1
Total	22	31	14	18	36	49

deployments depending on the lesion size. For each deployment, destruction was done in two cycles separated by 1 min of successive 10-W power increments every minute, from 50 W to 90 W or 75 % $\times$ 90 W, respectively, then maintained for 15 min. For all tumours, ablation was considered complete when the tumour was seen as a hyperechoic halo on real-time B-mode US monitoring with a 0.5–1-cm safety margin. No CEUS was performed during the procedure.

CA was done with Cryo-hit (Galil Medical, Ltd., Yokneam, Israel) using argon/helium gases with cryoprobe cooling based on the Joule-Thompson effect with high-pressure argon gas for freezing and pressurised helium gas for thawing. A 3-mm cryoprobe (Galil Medical, Ltd.) was inserted into the tumour under US guidance. For each probe location, two 10-min freeze–thaw cycles with a 5-min interfreezing thaw were performed. The progression of the front of the generated ice bulb was monitored with real-time US. The probe was then repositioned depending on the tumour size for additional two-cycle treatment sets to obtain a 0.5–1-cm safety margin surrounding the tumour in every dimension.

#### Imaging procedure

All CEUS examinations were performed with an Acuson Sequoia™ 512 (Siemens, Mountain View, CA) with a broadband 3–5-MHz transducer (4C1 Siemens). First, axial and sagittal pre-contrast gray-scale views of the treated areas were obtained. Second, non-linear imaging-mode Cadence™ contrast pulse sequencing (CPS) was used [16] after intravenous (IV) injection of 2.4 ml of SonoVue® (BR1, Bracco, Milan, Italy) [17]. As soon as the US contrast agent was administered, dual B-mode and CPS image sequences (17 frames/s) were acquired at a transmit frequency of 3 MHz with a low mechanical index of 0.17. From the arrival of the microbubbles in the imaging plane (arterial phase) until the end of the first minute after SonoVue® injection, several 3–5-s sweeps covering the whole treated zone in one plane were continuously recorded and saved as cine-loops on the hard drive of a separate computer.

Afterward, axial and sagittal images covering the ablated area were individually acquired every 30 s until 5-min post-injection. After 10 min, a second SonoVue® injection of 2.4 ml was given and a new sequence of image acquisitions was obtained covering the same treated area but in a perpendicular plane in order to assess the complete periphery of the treated area during the arterial phase. For each patient CEUS images were obtained once or less from day 1 to day 7 following ablation (T1), between weeks 3 and 6 (T2), week 7 and month 5 (T3), months 6 and 8 (T4), months 9 and 12 (T5), months 13 and 18 (T6), from month 19 to year 2 (T7) and during the third year post-treatment (T8). Two operators (AG, OL) with 2 and 7 years of experience with CEUS (at the beginning of the study), who were not blinded to treatment, performed all the CEUS during the study (Fig. 1).

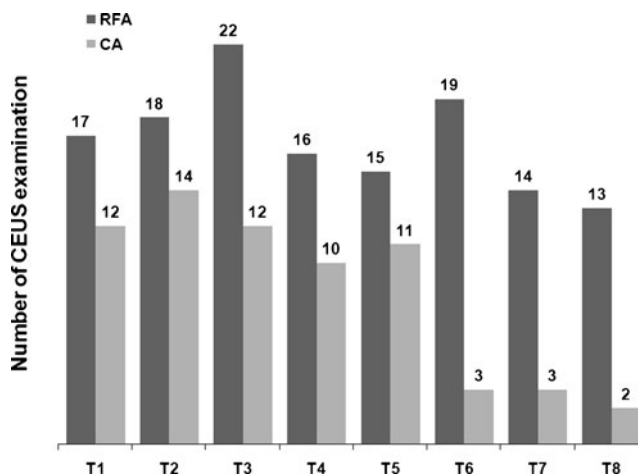


**Fig. 1** Distributions of the CEUS examinations performed during follow-up of the 31 RFA-treated lesions and the 18 CA-treated lesions. T1–T8 represent the different times during follow-up that CEUS was performed: T1: during week 1, days 1–7 following the ablation; T2: between weeks 3 and 6 following ablation; T3: between week 7 and month 5 after the treatment; T4: between months 6 and 8 post-ablation; T5: between months 9 and 12 post-treatment; T6: between months 13 and 18 after treatment; T7: between months 19 and 24 following ablation; T8: year 3 post-treatment

## CEUS analysis

Images and cine-loops were reviewed by consensus by three observers (C.B., A.G., O.L.). On the pre-contrast gray-scale images, the treated-zone pattern was defined as hypo-, iso- or hyperechoic, or alternating hypo- and hyperechoic. After contrast-agent injection, the treated-area margins on both cine-loops obtained during the arterial phase were described; the shape and volume of the devascularised area were evaluated on the images obtained during the portal and late phases. The margins were considered: “well defined” when the devascularised area exhibited sharp edges with the entire borders between non-enhancing and enhancing areas clearly delineated; “partially defined” when persistent small enhancing vessels penetrated into at least one portion of the periphery of the devascularised area and left at least one part of the periphery with a sharp edge (Fig. 2b); and “undefined” when the devascularised area edges were blurred because of persistent peripheral vessels penetrating into the treated zone that were visible along the whole periphery or in the entire treated area (Fig. 3b,c,d,f).

The large enhancing vessels passing through the devascularised area that were not destroyed by thermoablation were not considered. In addition, hyperenhancement of the area surrounding the treated area on the liver side during the arterial phases was noted and called the enhancing rim. This rim was considered thin when it was <3 mm thick all around the lesion on all sweeps (Fig. 2b) and thick when >3 mm (Fig. 3b) in at least one portion. The volume ( $V$ ) of the devascularised area was estimated from the axial and sagittal images passing through the largest diameter according to the following formula:  $V = a \times b \times c \times \pi/6$ , assuming an ellipsoid shape where  $a$ ,  $b$  and  $c$  represent the maximum diameters in the three dimensions of the treated zone.

## Statistical analysis

Percentages were compared with the chi-square test. When small numbers invalidated that approximation, the Yates correction was applied. The relationship between volumes of the devascularised areas and time was assessed using a

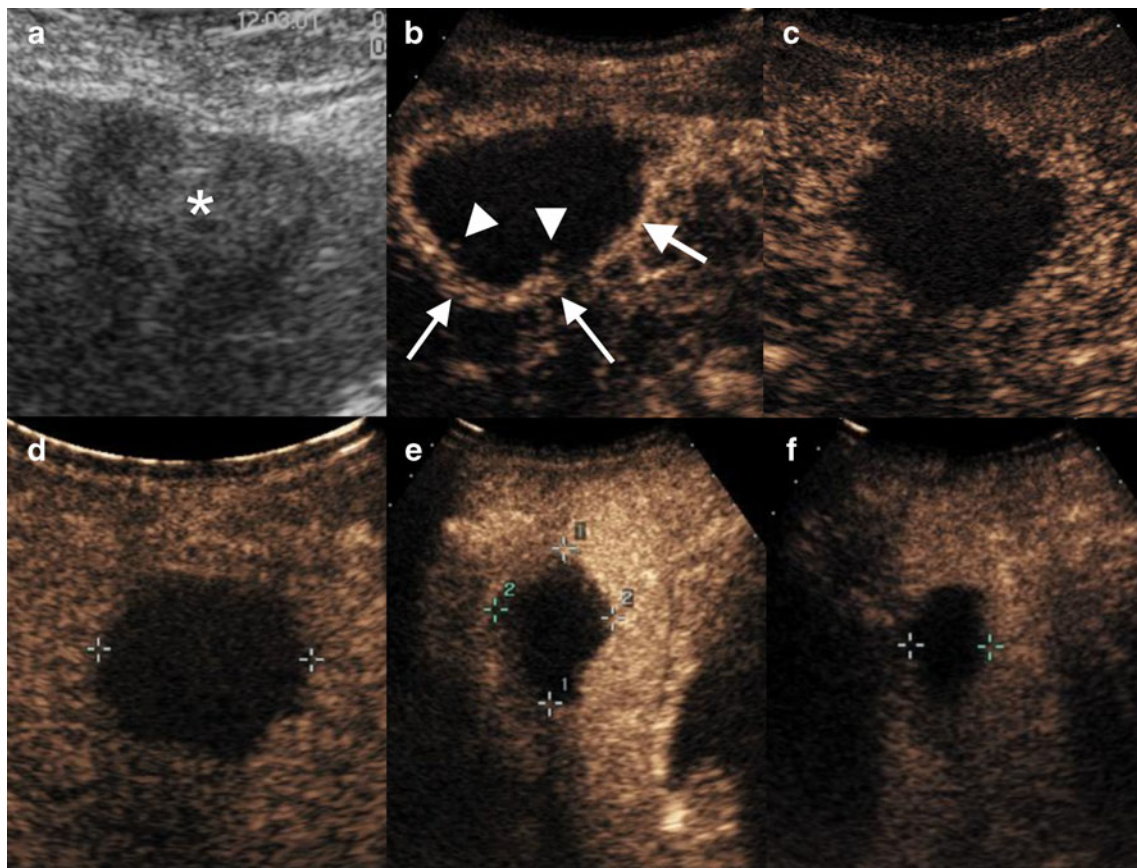


**Fig. 2** RF-induced lesion patterns. **a** T1 B-mode US obtained at D7 showed hypo- and hyperechoic areas. **b** T1 CEUS image obtained 18 s after contrast medium injection at D7 showed a thin enhancing rim (arrows) and a margin that was considered “partially defined” because peripheral small vessels penetrating into some portions of the devascularised area (arrowheads) are visible. **c** T2 CEUS image also

obtained 18 s after IV at week 4. The enhancing rim is no longer visible. The margin was still considered as partially defined. **d–f** CEUS images obtained during the late phase at T2 (120 s after IV injection at week 4), T4 (90 s after injection at month 6) and T6 (110 s after injection), respectively. The devascularised area volumes were calculated to be 48, 20 and 12 ml, respectively



mixed linear model, with the log-volume as dependent variable, thermoablative technique, time and thermoablative technique-time interaction as fixed effects, and lesion and lesion-time interaction as random effects. Significance was set at 5 % for the alpha error. Computations were performed using Statistical Analysis Software (SAS, Cary, NC).

## Results

Before injection of contrast medium, the B-mode pattern of the treated area was described according to the interval of time after treatment (Fig. 4). At (T2), RF lesions were easily identified because 24 % (4/17) were hypoechoic and 41 % (7/17) were hyperechoic, with only 12 % (2/17) isoechoic (Fig. 4a). At T4 and T7, respectively, 38 % (6/16) and 43 % (6/14) of the RF lesions had become difficult to distinguish from the surrounding liver parenchyma as they became isoechoic. Concerning cryolesions, 50 % (7/14) were hypoechoic, 7 % (1/14) hyperechoic and 43 % (6/14) isoechoic at T2 (Fig. 4b). After 1 year, 67 % (2/3) were isoechoic and difficult to discern. However, the differences between RF lesions and cryolesions did not reach the level of significance.

After contrast, at T1, 50 % (9/18) of the patients' RF-lesion margins were partially defined and 22 % (4/18) undefined (Fig. 5a). At T3, these patterns decreased with complete disappearance of the undefined pattern, while the percentage of RF lesions with partially defined margins declined regularly until T4 to reach 13 % (2/16). After month 8, the number of lesions with partially defined margins started to rise again to reach 54 % (7/13) after 3 years (T8).

At T1, 17 % (2/12) of patients' cryolesion margins were considered partially defined and 67 % (8/12) undefined (Fig. 5b). This pattern was more frequently encountered in cryolesions than in RF lesions ( $P < 0.02$ ). The percentage of undefined margins remained above 65 % through month 8. Small peripheral vessels remained visible in 66 % (2/3) of the cryolesions 1 and 2 years after CA, with margins considered partially defined in half the patients and undefined in the other half.

During the arterial phase, an enhancing rim surrounding the margins was seen at T1 in 28 % (5/18) and 75 % (9/12) of RF lesions and cryolesions, respectively ( $P < 0.02$ ). It was considered thin in 80 % (4/5) of RFA-treated patients, but thick in 89 % (8/9) of those treated with CA ( $P = 0.05$ ). At T2, the enhancing rim was still visible in 24 % (4/17) and 43 % (6/14) RFA- and CA-treated cases (NS), respectively. The rim was no longer visible 6 months after either thermoablative procedure.

For RF lesions, the mean volume of the devascularised area was a maximum of 1 week after the procedure ( $44.1 \pm 37.5$  ml) and shrank slowly over time, but the treated zone

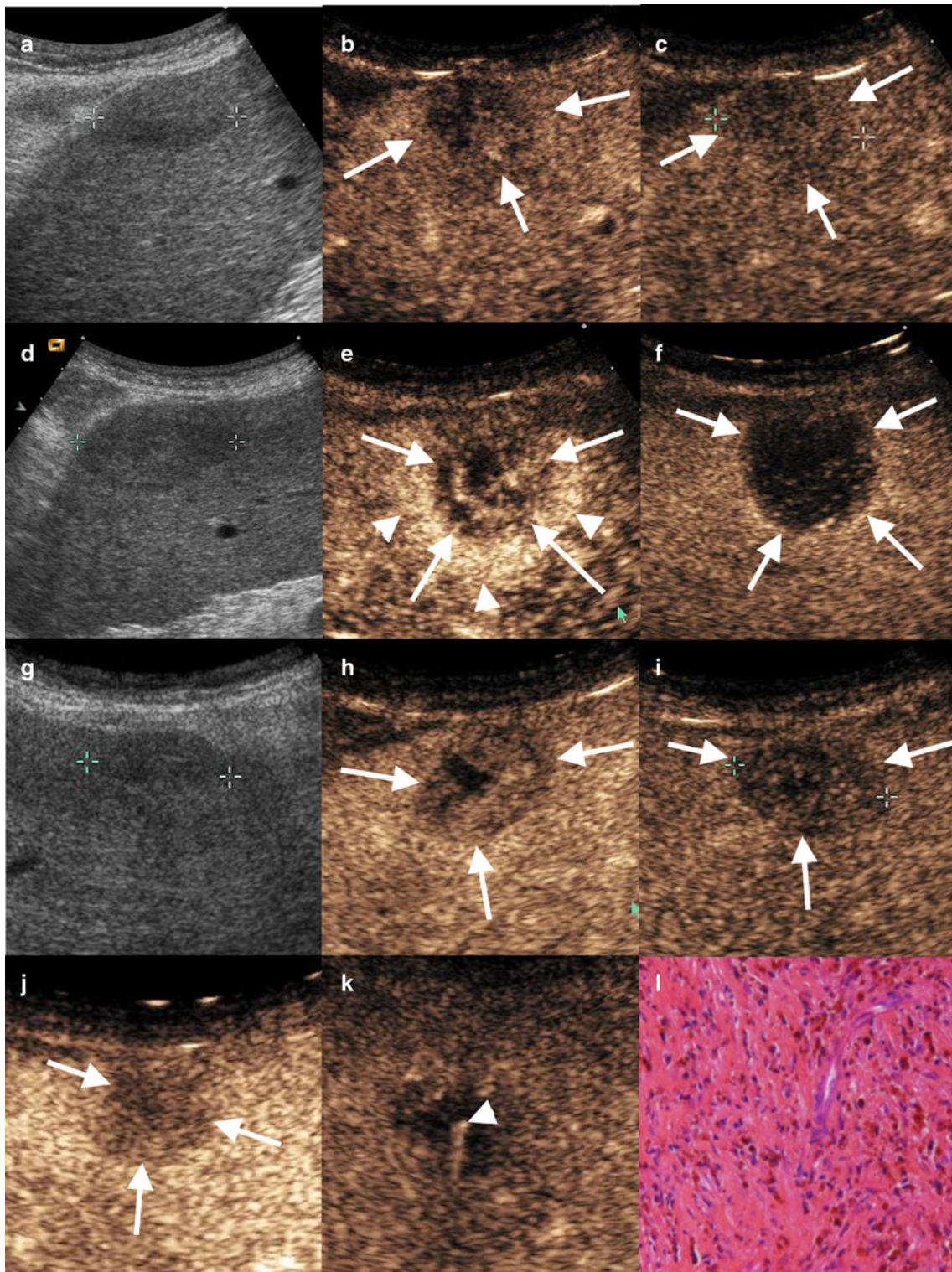
remained clearly visible  $>1$  year after ablation (average volume:  $8.3 \pm 7.4$  ml between months 13 and 18) (Fig. 6). The average T1 RF-lesion volume did not differ significantly between the non-cirrhotic ( $41.5 \pm 48.6$  ml) and cirrhotic livers ( $44.8 \pm 41.9$  ml) for comparable numbers of times the electrodes were unfolded (3.2 vs. 2.9 times, respectively). The CA-induced devascularised areas shrank over time from an average of  $16.6 \pm 7.1$  ml at T1 to  $1.7 \pm 1.3$  ml at T6 with a rate of shrinkage significantly faster than RF lesions ( $P = 0.009$ ).

## Discussion

CEUS is a technique highly sensitive to the presence of small amounts of microbubbles in the US field. In addition, microbubbles are true blood-pool agents that are consequently good markers of a tissue's vascular bed. Hence, CEUS is very sensitive to the presence of a residual functional vascular bed in a thermoablated area and can provide information about the vessels remaining in the treated zone. In this study, we focused only on successfully treated lesions to describe "normal" thermoablated zone patterns without the interference of possible residual tumour. We observed that, according to the thermoablation technique used, successfully treated areas behaved differently, and we considered these differences to be due to differences in the nature of thermal damage caused by RFA or CA.

RFA-induced thermal damage depends on the temperature achieved and the duration of heating. Near the electrode, immediate coagulation of tissue, including small vessels, is induced by temperatures between 60 °C and 100 °C. Further from the needle, where the temperature reaches 50–55 °C, the time needed to irreversibly damage cells is about 4–6 min, while, in the area heated to 45–55 °C, which could be considered a transition zone, this time ranges from 15 min (~54 °C) to several hours (~45 °C) [6, 15]. Because RFA must destroy 0.5–1 cm of normal tissue around the tumour margins [18], when treatment is successful, it is likely that the transition zone is located in the liver tissue. The temperature in this transition zone is expected to be heterogeneous because of the local tissue architecture and the heterogeneity of the blood flow that dissipates the heat via the bloodstream. Thus, in one part of the transition zone, the temperature might be just sufficient to destroy some capillaries with low flow rates, while in another part, the temperature is insufficient, leading to the persistence of viable capillaries.

In addition, outside and probably overlapping into the transition zone, the ablation process generates a rapid inflammatory reaction with granulation tissue, fibroblasts, inflammatory cells and capillary proliferation [19–21]. Both phenomena probably explain why we found 50 % partially



defined and 22 % undefined margins after contrast-agent injection at T1 after the procedure. The persistent peripheral small vessels leading to enhancement of the voxels that contain them could be either surviving vessels that escaped destruction or new vessels resulting from inflammatory

capillary proliferation. Zhou et al.'s observation [22] that the identification of the boundary of RF-ablated HCC was higher 15–22 h after RFA than 4 and 5 days later supports the last hypothesis. However, surviving vessels and inflammatory capillary proliferation cannot be distinguished in our



**Fig. 3** Post-CA cryolesion patterns of a biopsy-proven well-differentiated HCC. **a–c** Images obtained 1 day before the procedure. **a** On the B-mode, the lesion measured 3 cm at its longest diameter and appeared hypoechoic; its volume was estimated at 5 ml. **b** On CEUS 25 s after IV contrast-medium injection, the lesion (arrows) appeared rather hypovascularised with heterogeneous enhancement. **c** At 110 s after IV injection and later (not shown), the lesion was not clearly washed out. **d–f** T1 images obtained on D1 post-procedure. **d** On B-mode, a hypoechoic area measuring 4.3 cm at its longest diameter is seen (between calipers). **e** The CEUS image obtained 26 s after IV injection shows the persistence of numerous remaining enhancing vessels penetrating into the whole treated area (arrows) leading to classification of the margins as “undefined”. In addition, a thick enhancing rim (arrowheads) was also clearly visible. **f** At 110 s after IV injection, the treated area appeared more poorly vascularised than before cryoablation; its volume was calculated at 16 ml. **g–i** T3 images obtained at week 12 post-procedure. **g** On B-mode a hypoechoic area (between calipers) measuring 2.8 cm at its longest diameter is seen. **h** The CEUS image obtained 40 s after IV injection still showed undefined margins with persistence of numerous remaining enhancing vessels penetrating into the treated area (arrows) except a small central zone. The enhancing rim was no longer visible. **i** At 119 s after IV injection, the treated area appeared better vascularised than at T1; its volume was estimated at 7 ml. **j–l** T4 images obtained at month 6 post-ablation. **j** The CEUS image obtained 26 s after IV injection still shows undefined margins with persistent enhancing vessels penetrating into the whole treated area (arrows). **k** That observation led to a percutaneous CEUS-guided biopsy of the treated area to rule out incomplete treatment (the arrowhead shows the biopsy needle). **l** Histological examination found a hypervascular fibrosis without any tumour cells. The patient was followed for 2 additional years without recurrence

study because CEUS was not performed within minutes following the procedure but only during the first week thereafter, once the inflammatory reaction had probably already been established.

For the 28 % (5/18) well-defined margins the transition-zone heterogeneity could be undetectable, being too far below the spatial resolution of CEUS because of small differences between the temperatures reached or the weakness of the overlapping inflammatory reaction. The percentage of treated zones with partially or undefined margins decreased with time to reach a minimum at T4 (Fig. 5a) probably because of a clearance of inflammation and advanced tissue repair. However, after 8 months, the number of not well-defined margins tended to rise again, perhaps because of irregular RF-lesion shrinkage (see below).

We also saw a thin smooth enhancing rim in 28 % (5/18) of RFA-treated patients at T1 and 24 % (6/14) at T2. This enhancing rim probably reflects the inflammation-associated increase of local blood flow that occurs in vessels located outside the transition zone surrounding the RF lesion. This inflammatory process was strong enough to be seen with CEUS in 25 % of the patients and had to be differentiated from residual tumour, which usually exhibits a homogeneous crescent enhancement, different from a thin smooth enhancing rim. Because microbubbles remain strictly intravascular, CEUS is insensitive to the variation of vessel permeability induced by inflammation, which is usually responsible for the peripheral enhancement

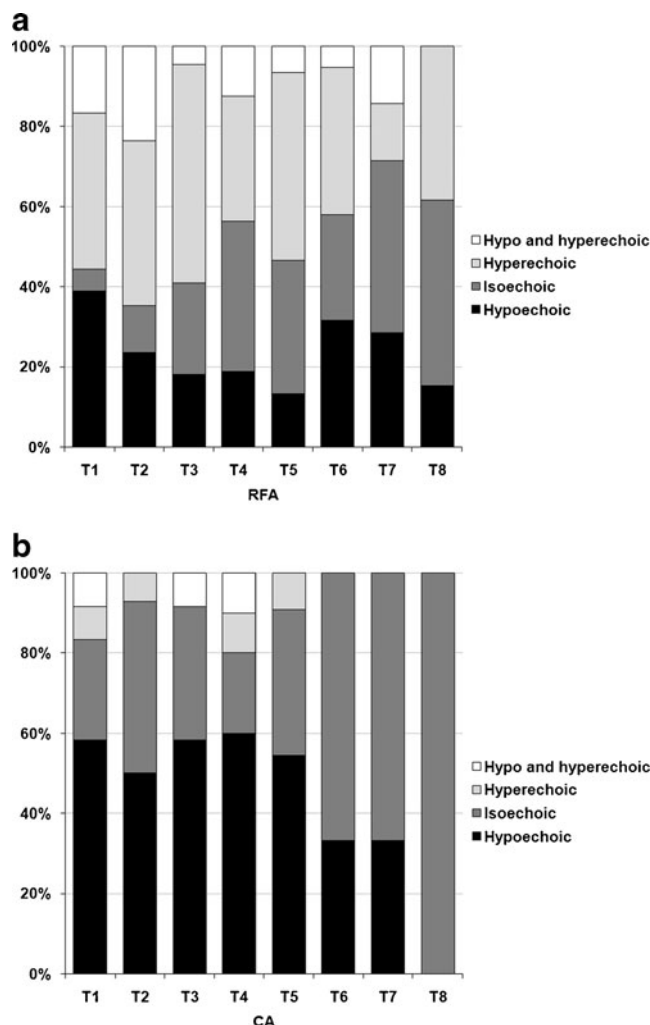


**Fig. 4** B-mode patterns of areas treated with RFA (a) or CA (b). See the legend Fig. 1 for time definitions

seen with the low-molecular-weight contrast compounds used in CT or MRI [23, 24]. This microbubble property might explain why an enhancing rim was described less often with CEUS in this study after RFA than in studies using CT, in which enhancing rims were seen in 89 % at 1 month and 22 % 3–6 months after RFA of HCC [25].

CA-induced thermal damage is the consequence of rapid freezing of tissues [26–29]. Close to the cryoprobe, the temperature rapidly achieves  $-190^{\circ}\text{C}$ , causing intra- and extracellular ice formation. Subsequent cell-membrane rupture during thawing and dehydration results in cell death. Further from the probe, where the temperature decreases more slowly, ice forms and propagates preferentially along the vascular system, within venules and arterioles, because cell walls impede intracellular ice crystal formation [27]. The resulting short-term hypoxia contributes to the death of surviving cells. However, it has been shown that canine large blood vessels were less sensitive to freezing injury than smaller vessels and bile ducts [30]. Consequently, at

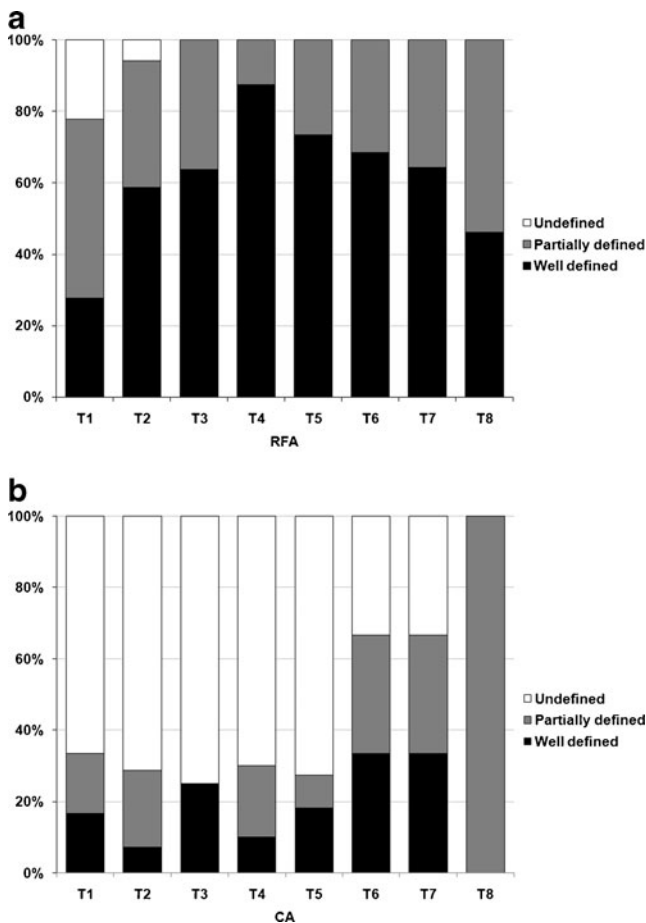


**Fig. 5** Contrast-enhanced patterns of the margins of the devascularised areas induced by RFA (a) or CA (b). See the legend in Fig. 1 for time definitions

the periphery of the treated area, more small capillaries are expected to be destroyed than larger vessels, creating a blurred transition zone. And like for RF lesions, an inflammatory reaction with granulation tissue occurs outside and probably overlapping the transition zone, as described

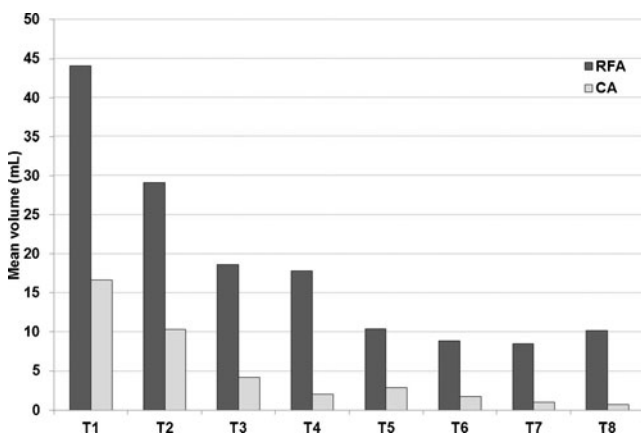


**Fig. 6** Mean volumes of the RF-induced lesions (RFA) and cryolesions (CA) and the evolution of their volumes over time

during histopathological analysis of cryolesions induced in rabbit livers 7 days after CA [21]. In that study, cryolesions, 15 mm in diameter, exhibited central coagulation necrosis with peripheral hepatic arterial and portal venous branches penetrating as much as 6 mm into the cryolesions, blood lakes similar to peliosis lesions and a peripheral 1–5-mm-thick rim of granulation tissue and inflammation [21]. Those histopathological features clearly correspond to our CEUS findings. Indeed, cryolesion margins were significantly less well defined at T1 than for RF lesions. Moreover, the enhancing rim was significantly thicker and more frequent around cryolesions than around RF lesions. On one hand, it is important to know that numerous peripheral small vessels that penetrate deep into a cryoablated area can persist after successful treatment. On the other hand, the persistence in 67 % (8/12) of the patients of such vascularisation, associated with the presence of a thick enhancing rim around this area, can preclude the identification of residual tumour, particularly a few days after the procedure.

Intriguingly, we also observed that the cryolesions shrank significantly faster than RF lesions. Matsumoto et al. [26] previously suggested, that RF-ablated kidney tumours do not regress in size the same way that cryoablated tumours do. The rapid shrinkage of the cryoablated lesions at as early as 3 months has been reported several times for renal tumours [31, 32], and the differences from the slower shrinkage of RF-ablated renal tumours has been explained by different treatment-induced histopathological lesions, mostly composed of necrotic tissue with intense macrophagic activity after CA [33] and with less necrosis but more granulomatous and fibrotic processes after RFA [34, 35]. We hypothesise that similar histopathological differences might occur in the liver with greater necrosis-resorption intensity (volume and rapidity) in the area of CA-induced coagulation necrosis than with RFA. This probably explains why it was often difficult to identify the CA-treated area on B-mode and even CEUS images more than 1 year after the procedure.

The main limitations of this study were the absence of histopathological analysis of the thermoablated areas and the fact that the observers who read the CEUS images were not blinded to the thermoablative technique used. However, in most cases two of the three observers did not know the treatment option and the readings were made by consensus, thereby limiting the risk of reading bias.

In conclusion, CEUS provided good visualisation of RFA- or CA-induced local modifications of the vascular bed, and good information about the vascularisation and the size of the transition zone between the totally destroyed area and the normal surrounding liver tissue. RF lesions and cryolesions appear to differ, particularly their margins and the rapidity of their shrinking. Our results indicate that, while RFA induces necrosis of tumour cells and blood vessels, CA could induce tumour-cell necrosis without



damaging a part of the intralesional microcirculation, at least at the periphery of most of the treated area. Knowledge about patterns of RFA- and CA-treated areas is essential for correct interpretation during CEUS follow-up.

**Acknowledgments** We would like to thank Jean Louis Golmard, MD, PhD, Department of Biostatistics, Université Paris 6–Pierre et Marie Curie, Paris, France, who did part of the statistical analysis.

## References

1. Buscarini L, Buscarini E, Di Stasi M, Vallisa D, Quaretti P, Rocca A (2001) Percutaneous radiofrequency ablation of small hepatocellular carcinoma: long-term results. *Eur Radiol* 11:914–921
2. Curley SA, Izzo F, Delrio P et al (1999) Radiofrequency ablation of unresectable primary and metastatic hepatic malignancies: results in 123 patients. *Ann Surg* 230:1–8
3. Khan MR, Poon RT, Ng KK et al (2007) Comparison of percutaneous and surgical approaches for radiofrequency ablation of small and medium hepatocellular carcinoma. *Arch Surg* 142:1136–1143, discussion 1143
4. Kerker S, Carlin AM, Sohn RL et al (2004) Long-term follow up and prognostic factors for cryotherapy of malignant liver tumors. *Surgery* 136:770–779
5. Paganini AM, Rotundo A, Barchetti L, Lezoche E (2007) Cryosurgical ablation of hepatic colorectal metastases. *Surg Oncol* 16:S137–S140
6. Goldberg SN, Gazelle GS, Mueller PR (2000) Thermal ablation therapy for focal malignancy: a unified approach to underlying principles, techniques, and diagnostic imaging guidance. *AJR Am J Roentgenol* 174:323–331
7. McGhana JP, Dodd GD 3rd (2001) Radiofrequency ablation of the liver: current status. *AJR Am J Roentgenol* 176:3–16
8. Ricci P, Cantisani V, Drudi F et al (2009) Is contrast-enhanced US alternative to spiral CT in the assessment of treatment outcome of radiofrequency ablation in hepatocellular carcinoma? *Ultraschall Med* 30:252–258
9. Vilana R, Bianchi L, Varela M et al (2006) Is microbubble-enhanced ultrasonography sufficient for assessment of response to percutaneous treatment in patients with early hepatocellular carcinoma? *Eur Radiol* 16:2454–2462
10. Shiozawa K, Watanabe M, Takayama R et al (2010) Evaluation of local recurrence after treatment for hepatocellular carcinoma by contrast-enhanced ultrasonography using Sonazoid: comparison with dynamic computed tomography. *J Clin Ultrasound* 38:182–189
11. Vilana R, Llovet JM, Bianchi L et al (2003) Contrast-enhanced power Doppler sonography and helical computed tomography for assessment of vascularity of small hepatocellular carcinomas before and after percutaneous ablation. *J Clin Ultrasound* 31:119–128
12. Frieser M, Kiesel J, Lindner A et al (2011) Efficacy of contrast-enhanced US versus CT or MRI for the therapeutic control of percutaneous radiofrequency ablation in the case of hepatic malignancies. *Ultraschall Med* 32:148–153
13. Bruix J, Sherman M (2005) Management of hepatocellular carcinoma. *Hepatology* 42:1208–1236
14. Chen MH, Yang W, Yan K et al (2004) Large liver tumors: protocol for radiofrequency ablation and its clinical application in 110 patients—mathematic model, overlapping mode, and electrode placement process. *Radiology* 232:260–271
15. Rhim H, Goldberg SN, Dodd GD 3rd et al (2001) Essential techniques for successful radio-frequency thermal ablation of malignant hepatic tumors. *Radiographics* 21:S17–S35, discussion S36–19
16. Phillips P, Gardner E (2004) Contrast-agent detection and quantification. *Eur Radiol* 14:P4–P10
17. Schneider M, Arditi M, Barrau MB et al (1995) BR1: a new ultrasonographic contrast agent based on sulfur hexafluoride-filled microbubbles. *Invest Radiol* 30:451–457
18. Morimoto M, Sugimori K, Shirato K et al (2002) Treatment of hepatocellular carcinoma with radiofrequency ablation: radiologic-histologic correlation during follow-up periods. *Hepatology* 35:1467–1475
19. Dromain C, de Baere T, Elias D et al (2002) Hepatic tumors treated with percutaneous radio-frequency ablation: CT and MR imaging follow-up. *Radiology* 223:255–262
20. Goldberg SN, Gazelle GS (2001) Radiofrequency tissue ablation: physical principles and techniques for increasing coagulation necrosis. *Hepatogastroenterology* 48:359–367
21. Kuszyk BS, Boitnott JK, Choti MA et al (2000) Local tumor recurrence following hepatic cryoablation: radiologic-histopathologic correlation in a rabbit model. *Radiology* 217:477–486
22. Zhou P, Kudo M, Minami Y et al (2007) What is the best time to evaluate treatment response after radiofrequency ablation of hepatocellular carcinoma using contrast-enhanced sonography? *Oncology* 72:92–97
23. Rhim H, Dodd GD 3rd (1999) Radiofrequency thermal ablation of liver tumors. *J Clin Ultrasound* 27:221–229
24. Smith S, Gillams A (2008) Imaging appearances following thermal ablation. *Clin Radiol* 63:1–11
25. Tsuda M, Majima K, Yamada T, Saitou H, Ishibashi T, Takahashi S (2001) Hepatocellular carcinoma after radiofrequency ablation therapy: dynamic CT evaluation of treatment. *Clin Imaging* 25:409–415
26. Matsumoto ED, Watumull L, Johnson DB et al (2004) The radiographic evolution of radio frequency ablated renal tumors. *J Urol* 172:45–48
27. Rubinsky B, Lee CY, Bastacky J, Onik G (1990) The process of freezing and the mechanism of damage during hepatic cryosurgery. *Cryobiology* 27:85–97
28. Shafir M, Shapiro R, Sung M, Warner R, Sicular A, Klipfel A (1996) Cryoablation of unresectable malignant liver tumors. *Am J Surg* 171:27–31
29. Shock SA, Laeseke PF, Sampson LA et al (2005) Hepatic hemorrhage caused by percutaneous tumor ablation: radiofrequency ablation versus cryoablation in a porcine model. *Radiology* 236:125–131
30. Gage AA, Fazekas G, Riley EE Jr (1967) Freezing injury to large blood vessels in dogs. With comments on the effect of experimental freezing of bile ducts. *Surgery* 61:748–754
31. Rodriguez R, Chan DY, Bishoff JT et al (2000) Renal ablative cryosurgery in selected patients with peripheral renal masses. *Urology* 55:25–30
32. Rukstalis DB, Khorsandi M, Garcia FU, Hoenig DM, Cohen JK (2001) Clinical experience with open renal cryoablation. *Urology* 57:34–39
33. Shingleton WB, Farabaugh P, Hughson M, Sewell PE Jr (2001) Percutaneous cryoablation of porcine kidneys with magnetic resonance imaging monitoring. *J Urol* 166:289–291
34. Johnson DB, Saboorian MH, Duchene DA, Ogan K, Cadeddu JA (2003) Nephrectomy after radiofrequency ablation-induced ureteropelvic junction obstruction: potential complication and long-term assessment of ablation adequacy. *Urology* 62:351–352
35. Zlotta AR, Wildschutz T, Raviv G et al (1997) Radiofrequency interstitial tumor ablation (RITA) is a possible new modality for treatment of renal cancer: ex vivo and in vivo experience. *J Endourol* 11:251–258